Water Splitting

International Edition: DOI: 10.1002/anie.201501616
German Edition: DOI: 10.1002/ange.201501616

Electrodeposited Cobalt-Phosphorous-Derived Films as Competent Bifunctional Catalysts for Overall Water Splitting**

*Nan Jiang, Bo You, Meili Sheng, and Yujie Sun**

Abstract: *One of the challenges to realize large-scale water splitting is the lack of active and low-cost electrocatalysts for its two half reactions: H_2 and O_2 evolution reactions (HER and OER). Herein, we report that cobalt-phosphorous-derived films (Co-P) can act as bifunctional catalysts for overall water splitting. The as-prepared Co-P films exhibited remarkable catalytic performance for both HER and OER in alkaline media, with a current density of 10 mA cm^{-2} at overpotentials of −94 mV for HER and 345 mV for OER and Tafel slopes of 42 and 47 mV/dec, respectively. They can be employed as catalysts on both anode and cathode for overall water splitting with 100 % Faradaic efficiency, rivalling the integrated performance of Pt and IrO_2. The major composition of the as-prepared and post-HER films are metallic cobalt and cobalt phosphide, which partially evolved to cobalt oxide during OER.*

Conversion of renewable energy resources through water splitting to H_2 and O_2 has attracted increasing attention.[1] The sluggish kinetics of H_2 and O_2 evolution reactions (HER and OER, respectively) necessitate the development of competent catalysts.[1] Owing to thermodynamic convenience and potential application in proton-exchange membrane or alkaline electrolyzers, most effort in this field has been devoted to developing HER catalysts for strongly acidic conditions and OER catalysts for strongly basic conditions. Transition-metal sulfides, selenides, phosphides, carbides, borides, and even non-metal materials have shown catalytic performance for HER in strong acidic electrolytes, such as MoS_2,[2] M-MoS_2,[3] Co/Ni-WS_x,[4] MS_2 and MSe_2 (M = Fe, Co, Ni, etc.),[5] FeS,[6] CoS,[7] Ni_3S_2,[8] MoC and MoB,[9] MoP,[10] WP and WP_2,[11] CoP and Co_2P,[12] Ni_2P,[13] FeP,[14] and Cu_3P.[15] On the other hand, many OER catalysts based on the oxides/hydroxides of cobalt,[16] nickel,[17] manganese,[18] iron,[19] and copper[20] have also been reported with OER catalytic activities under basic conditions. However, to accomplish overall water splitting, the coupling of HER and OER catalysts in the same electrolyte is desirable. The current prevailing approaches often result in incompatible integration of the two catalysts and lead to inferior overall performance. It remains a grand challenge to develop bifunctional electrocatalysts active for both HER and OER.

Herein, we report that a facile potentiodynamic electrodeposition using common cobalt and phosphorous reagents is able to prepare cobalt-phosphorous-derived (Co-P) films on copper foil (Figure S1 in the Supporting Information). The as-prepared Co-P films can be directly utilized as electrocatalysts for both HER and OER in strong alkaline electrolyte, which can achieve a current density of 10 mA cm^{-2} with overpotentials of −94 mV for HER and 345 mV for OER with very small Tafel slopes, 42 and 47 mV/dec, respectively. When the Co-P films were deposited on the anode and cathode for overall water splitting, the superior activity and stability of the catalytic films can even compete the integrated Pt and IrO_2 catalyst couple.

Scanning electron microscopy (SEM) images of the as-prepared Co-P film showed nearly complete coverage of the rough film on copper foil (Figure 1a and Figure S2). No crystalline particles or aggregates were observed. Elemental mapping analysis indicated Co and P were distributed evenly over the entire film (Figure S3). The cross section SEM image revealed the thickness of the film in 1–3 μm (Figure 1a inset and Figure S4). The X-ray photoelectron spectroscopy (XPS) survey of the as-prepared film (Figure S5) showed all the anticipated elements. The Co 2p XPS spectrum (Figure 1b) displayed two peaks at 778.3 and 793.4 eV, corresponding to the Co $2p_{3/2}$ and Co $2p_{1/2}$ binding energies, respectively.[21] These values are extremely close to those of metallic cobalt.[21] The P 2p XPS spectrum (Figure 1c) exhibits a dominant peak at 129.5 eV, which can be attributed to the phosphide signal.[21] A broad feature at approximately 133.6 eV is assigned to phosphate.[12b] In addition, elemental analysis of the as-prepared Co-P film gave the amount of Co and P as 2.52 and 0.19 mg cm^{-2}, respectively, with a molar ratio of 6.98 (Table S1).

We first evaluated the HER activity of the Co-P film in strong alkaline solution (Figure 2). It is evident that the blank copper foil did not show any HER catalytic activity before −0.3 V versus RHE (reversible hydrogen electrode). In contrast, a rapid cathodic current rise was observed for Co-P beyond −50 mV versus RHE (Figure 2a inset). Further scanning towards negative potential produced a dramatic increase in current density along with vigorous evolution of

[*] N. Jiang,[+] Dr. B. You,[+] M. Sheng, Dr. Y. Sun
Department of Chemistry and Biochemistry
Utah State University
0300 Old Main Hill, Logan, UT 84322 (USA)
E-mail: yujie.sun@usu.edu
Homepage: http://www.yujiesun.org

[+] These authors contributed equally to this work.

[**] N.J. acknowledges the Governor's Energy Leadership Scholars Grant of the State of Utah. This work was supported by Utah State University and the Principle Energy Issues Program of the State of Utah. We acknowledge the support from the Microscopy Core Facility at Utah State University for the SEM work. A provisional patent application by Y.S., N.J., and B.Y., has been filed for the intellectual property described in this communication. M.S. declares no competing financial interest.

Supporting information for this article is available on the WWW under http://dx.doi.org/10.1002/anie.201501616.

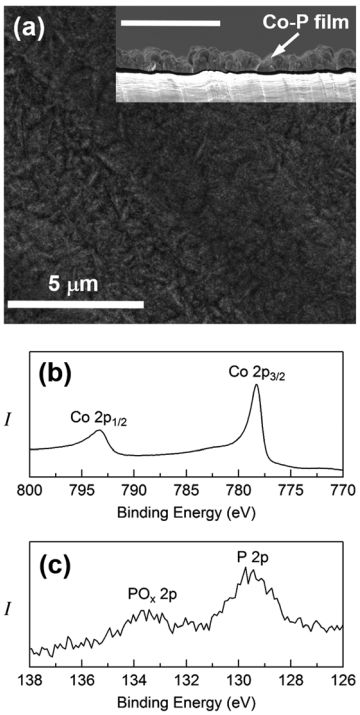

Figure 1. a) SEM image of an as-prepared Co-P film. Inset: the cross section of the Co-P film. Scale bars are both 5 μm. b),c) XPS spectra of an as-prepared Co-P film. b) Co 2p region, c) P 2p region.

H_2 bubbles from the electrode surface. The Co-P film required an overpotential (η) of only −94 mV to reach a current density of 10 mA cm^{-2}. Such a low overpotential requirement compares favorably to other reported HER catalysts at pH 14 (Table S2). Remarkably, the Co-P film was able to produce a catalytic current density of 1000 mA cm^{-2} within an overpotential of −227 mV. The linear fitting of its Tafel plot (Figure 2b) gave a Tafel slope of 42 mV/dec, which is among the smallest Tafel slopes of reported HER catalysts in alkaline media (Table S2). Although Pt-C exhibited a very small catalytic onset potential, its Tafel slope (108 mV/dec) was significantly larger than that of the Co-P film. Therefore, beyond −167 mV versus RHE, the catalytic current density of Co-P surpassed that of Pt-C. Additionally, the Co-P film also exhibited superior long-term stability. A 24 h controlled potential electrolysis at $\eta = -107$ mV showed a nearly linear charge accumulation and steady current over the entire course of electrolysis (Figure 2c). The blank copper foil generated negligible charge build-up under the same condition.

To probe the morphology and composition of the Co-P film after HER electrocatalysis, the SEM and XPS results of a post-HER Co-P film were collected. As shown in Figure 2d, the film still maintained a uniform coverage on the copper foil and no apparent clusters or aggregates were observed (Figure S6). Elemental mapping analysis confirmed the even distribution of Co and P in the post-HER film (Figure S7). Its Co 2p XPS spectrum showed two peaks at 793.2 and 778.2 eV (Figure 3a), corresponding to Co $2p_{3/2}$ and Co $2p_{1/2}$ states, respectively. The similarity of the Co 2p peaks of the post-HER Co-P film compared to those of the as-prepared one (Figure 1b) implied the major composition of the film preserved as metallic cobalt during HER. Furthermore, a peak at 129.3 eV was observed from the P 2p XPS spectrum of the post-HER sample (Figure 3b); while the phosphate peak at 133.6 eV originally observed for the as-prepared Co-P film (Figure 1c) was absent. Its absence is likely due to the dissolution of cobalt phosphate under cathodic condition. As shown in Figure S9, the as-prepared and post-HER Co-P films exhibited similar capacitance, implying their similar electrical active surface area. Elemental analysis of the post-HER film gave Co and P amounts of 2.48 and 0.12 mg cm^{-2} with a Co/P ratio of 10.5 (Table S1).

We next assessed the catalytic activity of the Co-P film for OER in the same electrolyte (Figure 4). As expected, a blank copper did not show appreciable anodic current before 1.7 V versus RHE. The OER catalytic current density of the Co-P film increased dramatically beyond 1.53 V versus RHE (Figure 4a inset). It could reached current densities of 10, 100, and 500 mA cm^{-2} at $\eta = 345$, 413, and 463 mV, respectively, lower than those of IrO_2 and many other reported OER catalysts (Table S3). Linear fitting of its Tafel plot resulted in a Tafel slope of 47 mV/dec. As one of the state-of-the-art OER catalysts,

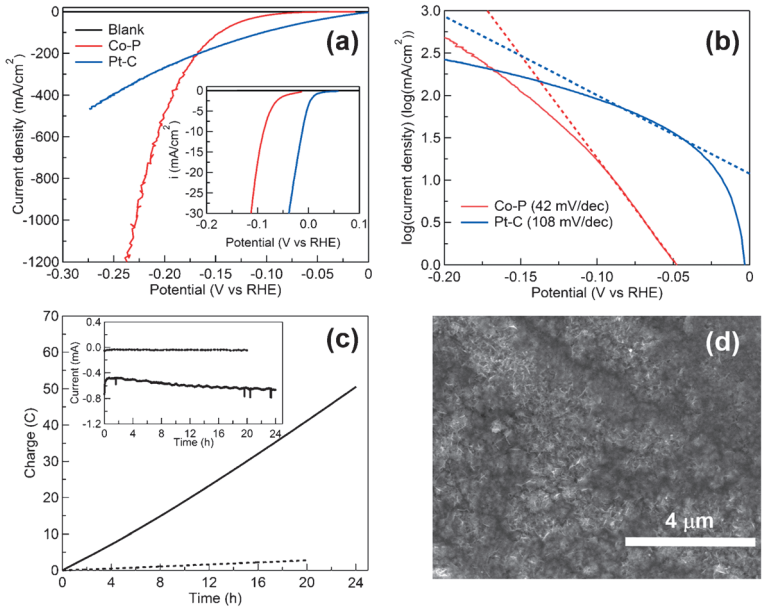

Figure 2. a) Polarization curves of Co-P (red), Pt/C (blue), and blank Cu foil (black) in 1 M KOH at scan rate of 2 mV s^{-1} and rotating rate of 2000 rpm (Inset: expanded region around the onsets of the polarization curves); b) corresponding Tafel plots of Co-P/Cu film (red), Pt/C (blue) with their associated linear fittings (dotted lines); c) long-term controlled potential electrolysis of Co-P (solid) and blank Cu foil (dotted) in 1 M KOH at an overpotential of 107 mV (Inset: the corresponding current change over time of Co-P (bottom trace) and blank Cu foil (top trace) during the electrolysis); d) SEM image of Co-P after 2 h H_2 evolution electrolysis at $\eta = -107$ mV.

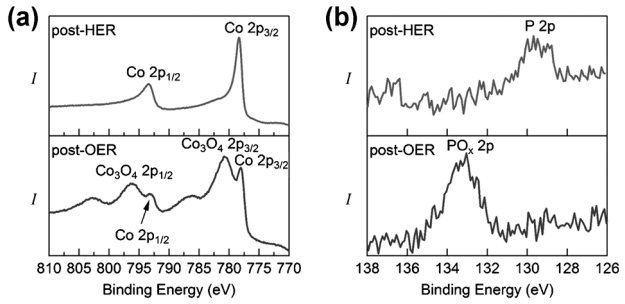

Figure 3. XPS spectra of a) Co 2p and b) P 2p regions of Co-P films after HER (top) or OER (bottom) electrolyses.

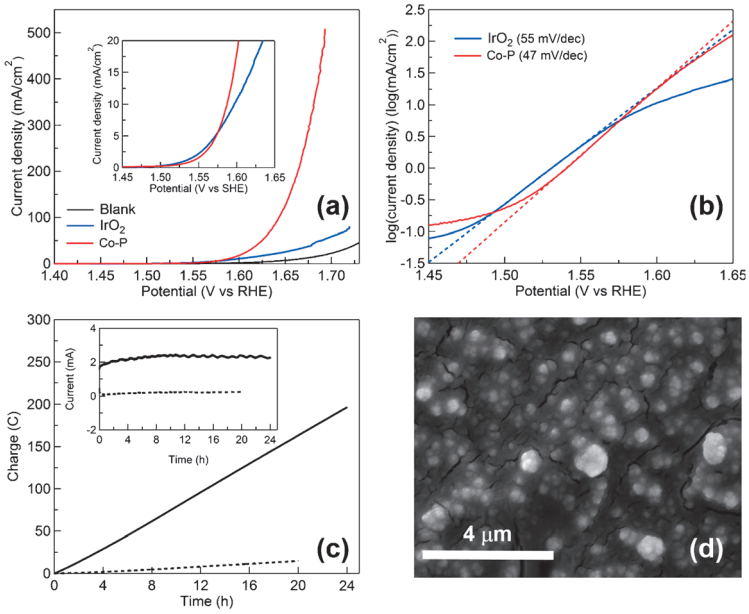

Figure 4. a) Polarization curves of Co-P (red), IrO_2 (blue), and blank Cu foil (black) in 1 M KOH at scan rate of 2 $mV s^{-1}$ and rotating rate of 2000 rpm (Inset: the expanded region around the onsets of the polarization curves of Co-P and IrO_2; b) corresponding Tafel plots of Co-P (red) and IrO_2 (blue) with their associated linear fittings (dotted lines); c) long-term controlled potential electrolysis of Co-P (solid) and blank Cu foil (dotted) in 1 M KOH at an overpotential of 343 mV (Inset: the corresponding current change over time of Co-P (solid) and blank Cu foil (dotted) during the electrolysis); d) SEM image of Co-P after a 2 h OER electrolysis at $\eta = 343$ mV.

IrO_2 was able to catalyze OER at a lower onset of approximately 1.50 V versus RHE, however its performance was quickly exceeded by that of the Co-P film beyond 1.58 V versus RHE. In fact, the Tafel slope of Co-P (47 mV/dec) is even lower than that of IrO_2 (55 mV/dec), demonstrating more favorable OER kinetics of the Co-P. Besides high OER activity, the Co-P film also features excellent stability, as revealed by a 24 h controlled potential electrolysis at $\eta =$ 343 mV (Figure 4c).

The SEM image (Figure 4d) of the post-OER Co-P film indicates it contains large nanoparticle aggregates, in sharp contrast to the rough and porous morphology of the as-prepared and post-HER samples (Figure 1a and Figure 2d). Nevertheless, elemental mapping analysis still demonstrated the even distribution of Co and P in the film (Figure S11), plus a large concentration of O. Indeed, an intense O 1s peak was observed in the XPS survey spectrum of the post-OER film (Figure S12). The Co 2p spectrum displayed two peaks at 780.7 and 796.3 eV (Figure 3a), which can be assigned to oxidized cobalt, Co_3O_4, plus its satellite peaks at 786.3 and 802.7 eV.[12b] However, the metallic cobalt 2p peaks at 778.0 and 793.0 eV could still be well resolved. The P 2p spectrum showed a phosphate peak at 133.2 eV (Figure 3b), whereas the original phosphide feature at 129.5 eV disappeared completely. Taken together, it indicated that the original cobalt in the Co-P film was partially oxidized to Co_3O_4 and cobalt phosphate during OER. An OER electrocatalyst with a metallic cobalt core and cobalt oxide/hydroxide shell was reported.[22] Elemental analysis of the post-OER film resulted in the remaining amount of Co and P as 2.47 and 0.13 mg cm^{-2} with a Co/P ratio of 9.74 (Table S1), still similar to those of the post-HER film.

Based on the results aforementioned, we anticipated that the Co-P film could act as a bifunctional electrocatalyst for overall water splitting. Hence, a two-electrode configuration was employed (Figure 5a). When the as-prepared Co-P films were used as electrocatalysts for both anode and cathode (Co-P/Co-P couple), a catalytic current was observed when the applied potential was larger than 1.56 V with a Tafel slope of 69 mV/dec.The rapid catalytic current density exceeded 100 mA cm^{-2} at 1.744 V. When Pt-C or IrO_2 was used for both electrodes (Pt-C/Pt-C or IrO_2/IrO_2 couple), much diminished catalytic current densities were obtained with large Tafel slopes of 166 and 290 mV/dec, respectively. Since Pt is well-established for HER and IrO_2 for OER, the integration of Pt-C on cathode and IrO_2 on anode was expected to produce the excellent catalytic system. Indeed, the IrO_2/Pt-C couple was able to catalyze water splitting with an onset around 1.47 V (Figure 5a inset). However, the Tafel slope of IrO_2/Pt-C is 91 mV/dec, larger than that of Co-P/Co-P (69 mV/dec). Therefore, when the applied potential was higher than 1.67 V, Co-P/Co-P was able to surpass IrO_2/Pt-C in catalyzing overall water splitting. In addition, the Co-P/Co-P couple maintained excellent stability as manifested by the steady current change and nearly linear charge accumulation for a 24 h electrolysis (Figure 5c). In fact, the integrated activity of IrO_2/Pt-C was slightly inferior to that of the Co-P/Co-P couple under the same conditions. Figure 5d indicates the produced H_2 and O_2 quantified by gas chromatography match the calculated amount based on passed charge well and the volume ratio of H_2 and O_2 is close to 2, leading to a Faradaic efficiency of 100%.

In conclusion, we have reported electrodeposited Co-P films can act as bifunctional catalysts for overall water splitting. The catalytic activity of the Co-P films can rival the state-of-the-art catalysts, requiring $\eta = -94$ mV for HER and $\eta = 345$ mV for OER to reach 10 mA cm^{-2} with Tafel

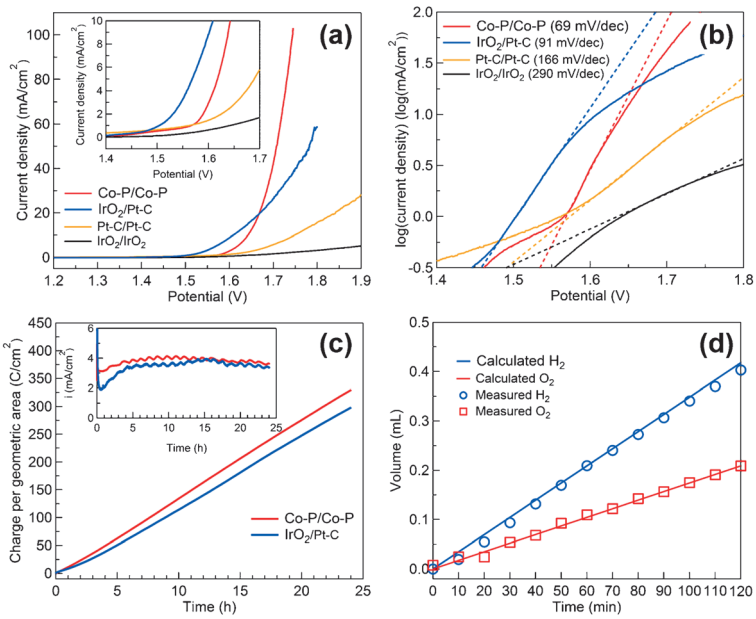

Figure 5. a) Polarization curves of Co-P/Co-P (red), IrO_2/Pt-C (blue), Pt-C/Pt-C (yellow), and IrO_2/IrO_2 (black) for overall water splitting in 1 M KOH at a scan rate of 2 $mV s^{-1}$ (Inset: the expanded region around the onsets of those polarization curves); b) corresponding Tafel plots of Co-P/Co-P (red), IrO_2/Pt-C (blue), Pt-C/Pt-C (yellow), and IrO_2/IrO_2 (black) and their associated linear fittings (dotted lines); c) long-term controlled potential electrolysis of Co-P (red) and IrO_2/Pt-C (blue) in 1 M KOH at an overpotential of 400 mV (Inset: the corresponding current change over time of Co-P (red) and IrO_2/Pt-C (blue)); d) generated H_2 and O_2 volumes over time versus theoretical quantities assuming a 100% Faradaic efficiency for the overall water splitting of Co-P/Co-P in 1 M KOH at $\eta = 400$ mV.

slopes of 45 and 47 mV/dec, respectively. It can be directly utilized as catalysts for both anode and cathode with superior efficiency, strong robustness, and 100% Faradaic yield. The understanding of real-time composition and structural evolution of the films during electrolysis requires in situ spectroscopic study, which is under current investigation.

Keywords: electrocatalysts · nonprecious metal catalysts · overall water splitting · potentiodynamic deposition

How to cite: *Angew. Chem. Int. Ed.* **2015**, *54*, 6251–6254
Angew. Chem. **2015**, *127*, 6349–6352

[1] a) H. B. Gray, *Nat. Chem.* **2009**, *1*, 7; b) T. R. Cook, D. K. Dogutan, S. Y. Reece, Y. Surendranath, T. S. Teets, D. G. Nocera, *Chem. Rev.* **2010**, *110*, 6474–6502; c) M. G. Walter, E. L. Warren, J. R. McKone, S. W. Boettcher, Q. Mi, E. A. Santori, N. S. Lewis, *Chem. Rev.* **2010**, *110*, 6446–6473.

[2] a) T. F. Jaramillo, K. P. Jorgensen, J. Bonde, J. H. Nielsen, S. Horch, I. Chorkendorff, *Science* **2007**, *317*, 100–102; b) D. Merki, S. Fierro, H. Vrubel, X. L. Hu, *Chem. Sci.* **2011**, *2*, 1262–1267; c) C. G. Morales-Guio, X. L. Hu, *Acc. Chem. Res.* **2014**, *47*, 2671–2681.

[3] D. Merki, H. Vrubel, L. Rovelli, S. Fierro, X. L. Hu, *Chem. Sci.* **2012**, *3*, 2515–2525.

[4] P. D. Tran, S. Y. Chiam, P. P. Boix, Y. Ren, S. S. Pramana, J. Fize, V. Artero, J. Barber, *Energy Environ. Sci.* **2013**, *6*, 2452–2459.

[5] D. Kong, J. J. Cha, H. Wang, H. R. Lee, Y. Cui, *Energy Environ. Sci.* **2013**, *6*, 3553–3558.

[6] C. Di Giovanni, W. A. Wang, S. Nowak, J. M. Grenèche, H. Lecoq, L. Mouton, M. Giraud, C. Tard, *ACS Catal.* **2014**, *4*, 681–687.

[7] a) Y. Sun, C. Liu, D. C. Grauer, J. Yano, J. R. Long, P. Yang, C. J. Chang, *J. Am. Chem. Soc.* **2013**, *135*, 17699–17702; b) B. You, N. Jiang, M. L. Sheng, Y. Sun, *Chem. Commun.* **2015**, *51*, 4252–4255.

[8] N. Jiang, L. Bogoev, M. Popova, S. Gul, J. Yano, Y. Sun, *J. Mater. Chem. A* **2014**, *2*, 19407–19414.

[9] a) H. Vrubel, X. Hu, *Angew. Chem. Int. Ed.* **2012**, *51*, 12703–12706; *Angew. Chem.* **2012**, *124*, 12875–12878; b) L. Liao, S. Wang, J. Xiao, X. Bian, Y. Zhang, M. D. Scanlon, X. Hu, Y. Tang, B. Liu, H. H. Girault, *Energy Environ. Sci.* **2014**, *7*, 387–392.

[10] Z. Xing, Q. Liu, A. M. Asiri, X. P. Sun, *Adv. Mater.* **2014**, *26*, 5702–5707.

[11] a) J. M. McEnaney, J. Chance Crompton, J. F. Callejas, E. J. Popczun, C. G. Read, N. S. Lewis, R. E. Schaak, *Chem. Commun.* **2014**, *50*, 11026–11028; b) Z. Xing, Q. Liu, A. M. Asiri, X. P. Sun, *ACS Catal.* **2015**, *5*, 145–149.

[12] a) E. J. Popczun, C. G. Read, C. W. Roske, N. S. Lewis, R. E. Schaak, *Angew. Chem. Int. Ed.* **2014**, *53*, 5427–5430; *Angew. Chem.* **2014**, *126*, 5531–5534; b) F. H. Saadi, A. I. Carim, E. Verlage, J. C. Hemminger, N. S. Lewis, M. P. Soriaga, *J. Phys. Chem. C* **2014**, *118*, 29294–29300; c) Z. Pu, Q. Liu, P. Jiang, A. M. Asiri, A. Y. Obaid, X. P. Sun, *Chem. Mater.* **2014**, *26*, 4326–4329.

[13] E. J. Popczun, J. R. McKone, C. G. Read, A. J. Biacchi, A. M. Wiltrout, N. S. Lewis, R. E. Schaak, *J. Am. Chem. Soc.* **2013**, *135*, 9267–9270.

[14] a) Y. Xu, R. Wu, J. Zhang, Y. Shi, B. Zhang, *Chem. Commun.* **2013**, *49*, 6656–6658; b) P. Jiang, Q. Liu, Y. Liang, J. Q. Tian, A. M. Asiri, X. P. Sun, *Angew. Chem. Int. Ed.* **2014**, *53*, 12855–12859; *Angew. Chem.* **2014**, *126*, 13069–13073.

[15] J. Q. Tian, Q. Liu, N. Cheng, A. M. Asiri, X. P. Sun, *Angew. Chem. Int. Ed.* **2014**, *53*, 9577–9581; *Angew. Chem.* **2014**, *126*, 9731–9735.

[16] a) M. W. Kanan, D. G. Nocera, *Science* **2008**, *321*, 1072–1075; b) J. Feng, F. Heinz, *Energy Environ. Sci.* **2010**, *3*, 1018–1027.

[17] M. Dinca, Y. Surendranath, D. G. Nocera, *Proc. Natl. Acad. Sci. USA* **2010**, *107*, 10337–10341.

[18] a) I. Zaharieva, M. M. Najafpour, M. Wiechen, M. Haumann, P. Kurz, H. Dau, *Energy Environ. Sci.* **2011**, *4*, 2400–2408; b) F. Song, X. L. Hu, *J. Am. Chem. Soc.* **2014**, *136*, 16481–16484.

[19] a) R. D. L. Smith, M. S. Prévot, R. D. Fagan, Z. Zhang, P. A. Sedach, M. K. J. Siu, S. Trudel, C. P. Berlinguette, *Science* **2013**, *340*, 60–63; b) D. Friebel, M. W. Louie, M. Bajdich, K. E. Sanwald, Y. Cai, A. M. Wise, M. J. Cheng, D. Sokaras, T. C. Weng, R. Alonso-Mori, R. C. Davis, J. R. Bargar, J. K. Nørskov, A. Nilsson, A. T. Bell, *J. Am. Chem. Soc.* **2015**, *137*, 1305–1313.

[20] J. Du, Z. Chen, S. Ye, B. J. Wiley, T. J. Meyer, *Angew. Chem. Int. Ed.* **2015**, *54*, 2073–2078; *Angew. Chem.* **2015**, *127*, 2101–2106.

[21] A. P. Grosvenor, S. D. Wik, R. G. Cavell, A. Mar, *Inorg. Chem.* **2005**, *44*, 8988–8998.

[22] S. Cobo, J. Heidkamp, P.-A. Jacques, J. Fize, V. Fourmond, L. Guetaz, B. Jousselme, V. Ivanova, H. Dau, S. Palacin, M. Fontecave, V. Artero, *Nat. Mater.* **2012**, *11*, 802–807.

Received: February 18, 2015
Published online: April 20, 2015

